ELSEVIER

Journal of Nuclear Materials 240 (1997) 229–235

journal of nuclear materials

Microstructural study of an irradiated high-nickel alloy by X-ray line profile analysis and TEM observations

R.B. Grabova *, V.K. Gorbatov, Z.E. Ostrovsky, R.A. Yuskaev

State Scientific Centre of Russia, Research Institute of Atomic Reactors, Ulyanovsk Region, 433510 Dimitrovgrad 10, Russia

Received 24 February 1996; accepted 16 September 1996

Abstract

The microstructure was investigated in previously deformed specimens of a high-nickel alloy with four levels of initial dislocation density, both before and after irradiation in BOR-60 reactor at 370–400°C and three displacement rates. The network dislocation density, dislocation loop radius and loop number density were determined by both X-ray line profile analysis and TEM observations. The dependence of dislocation structure parameters on irradiation conditions and initial network density was obtained.

1. Introduction

Presently, many intensive studies of the influence of dose rate and neutron spectral effects on the behavior of structural materials for various types of reactors are being carried out. Significant experimental data concerning the influence of reactor irradiation parameters on swelling, in-reactor creep and radiation induced changes in tensile properties of materials are now available [1,2]. However, there are only a few data concerning the influence of irradiation variables on dislocation structure evolution [3,4].

Microstructural changes in irradiated materials traditionally are investigated using transmission electron microscopy (TEM). Its accuracy is limited by the following factors: foil thickness measurement error, possible dislocation loss during and after foil preparation, local heterogeneity of dislocation structure and limited resolution for dislocation densities higher than 10^{15} m^{-2}.

X-ray studies of irradiated or deformed materials do not require such specimen thinning before examination and therefore allow us to determine bulk-averaged microstructure levels. The theory of X-ray scattering by imperfect crystals [5] provides quantitative relations between microstructural components and X-ray scattering effects. On the basis of these relationships the measurements of network dislocation density have been performed for plastically deformed metals and alloys [6,7]. Dislocation loop parameters have been determined in our laboratory for both irradiated Ni [8] and Mo [9].

Microstructure of structural materials irradiated up to the high doses at elevated temperatures is composed of various components, and therefore may yield a complicated profile of X-ray lines.

The purpose of this current work consists of the following:

– development of procedures and software to calculate microstructural parameters of both irradiated and deformed materials by X-ray line (XRL) profile analysis;

– microstructural studies of deformed specimens of high-nickel alloy (type 20Cr–45Ni) with different initial dislocation densities before and after irradiation in the BOR-60 fast reactor at three displacement rate levels;

– comparison of the microstructural study results obtained by both XRL profile analysis and TEM observation;

– determination of microstructural parameter dependence on irradiation conditions and initial dislocation density.

* Corresponding author. Fax: +7-84235 35 648.

PII S0022-3115(96)00678-2

2. Principles of X-ray studies of irradiated materials

According to the theory of X-ray scattering by imperfect crystals [5], various components of the microstructure of irradiated and/or deformed materials involve different X-ray scattering mechanisms, that define the X-ray line intensity distribution. Dislocation loops or precipitates of a new phase create a Coulomb displacement field that causes a shift and a decrease in intensity of the Bragg reflection peaks, yielding a diffuse X-ray scattering. The intensity distribution, $I(2\theta)$, considered as a function of scattering angle 2θ can be presented by

$$I(2\theta) = I_{0i}\delta\left(2\theta - 2\theta_m^0\right) + I_1(2\theta), \tag{1}$$

where the δ-function represents the Bragg reflection peak, with integral intensity I_{0i} and position $2\theta_m^0$, and $I_1(2\theta)$ describes the diffuse scattering intensity distribution, where

$$I_{0i} = (I_{0i} + I_{1i})e^{-2M}, \tag{2}$$

I_{1i} is the diffuse scattering integral intensity and M depends on the defect concentration, type and size. For cubic symmetry defects creating a net radial displacement field, $\boldsymbol{u}(\boldsymbol{r}) = C\boldsymbol{r}/r^3$, in cubic elastically-isotropic crystals [10]

$$M = \frac{4\pi}{3}N(|C|Q)^{3/2}, \tag{3}$$

where $Q = (4\pi/\lambda)\sin\theta$, λ is X-ray wavelength, N is the defect density, and the parameter C defines the crystal volume change due to defect introduction. For interstitial loops and precipitates which expand the lattice, $C > 0$. The shift of the Bragg reflection peak with respect to position for perfect crystal, $2\theta_0^0$, is determined by

$$2\left(\theta_m^0 - \theta_0^0\right) = -\frac{8\pi}{3}\left(1 + 2\frac{1-2\nu}{1-\nu}\right)NC\tan\theta, \tag{4}$$

where ν is Poisson's factor.

The shape of the diffuse scattering intensity distribution depends on $2M$. For $2M \approx 1$, when X-ray lines have doublet structure, the distribution $I_1(2\theta)$ is significantly asymmetric, but the asymmetry decreases with an increase in M. The integral width of intensity distribution, $2\delta\theta_i$, and the shift of its maximum, $2(\theta_m - \theta_0^0)$, are described by

$$2\delta\theta_i = \frac{8\pi}{3}\eta_i N|C|\tan\theta, \tag{5}$$

$$2\left(\theta_m - \theta_0^0\right) = \frac{8\pi}{3}\left(\eta_m - 2\frac{1-2\nu}{1-\nu}\right)NC\tan\theta, \tag{6}$$

where η_i and η_m are functions of $2M$. In Fig. 1 are shown the calculated dependencies for results obtained in Ref. [10], according to which both the integral width and shift of diffuse scattering maximum significantly increase at $2M \to 0$. When $2M \gg 1$, the intensity of the Bragg reflection vanishes and the diffuse scattering profile is described by a Cauchy distribution

$$I_1(2\theta) = \frac{I_{1i}}{\pi}\frac{\sigma_c}{\sigma_c^2 + (2\theta - 2\theta_m)^2}, \tag{7}$$

where $\sigma_c = 2\delta\theta_i/\pi$.

The relationships presented above can be used for the description of X-ray scattering by irradiated materials which contain dislocation loops. According to Ref. [11] for Frank loops randomly oriented on {111} planes in elastically-isotropic fcc crystals, C can be estimated by

$$C = \frac{1}{12\sqrt{3}}\frac{1+\nu}{1-\nu}aR^2, \tag{8}$$

where R is the radius of loops, and a is the lattice parameter. If there are both large and small loops of interstitial and vacancy type, then by Ref. [5] the value of M, the magnitude and direction of Bragg reflection shift are determined by additive contributions of various type defects. Due to the strong M dependence on loop size ($M \sim R^3$), the diffuse scattering characteristics are to be determined largely by loops of the greatest size.

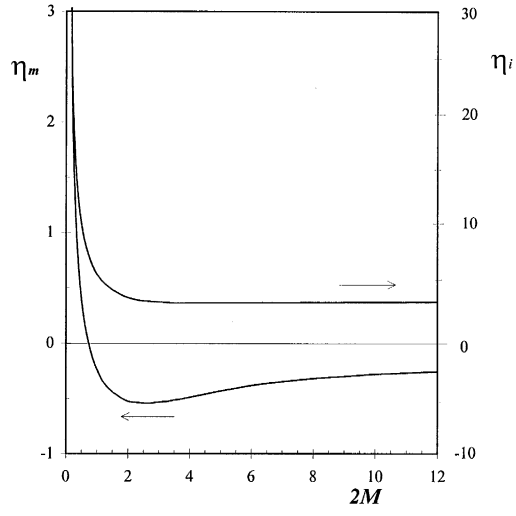

Fig. 1. Function for calculation of maximum position and integral width of diffuse scattering intensity distribution.

The X-ray scattering by crystals containing randomly distributed line dislocations (in the absence of defects of other types) leads to Bragg reflection broadening, that is determined by the dislocation density. For plastically-deformed metals and alloys, the broadening may be described by a square Cauchy distribution [6]

$$C^2(2\theta) = \frac{2\sigma_n^3}{\pi}\frac{1}{\left[\sigma_n^2 + \left(2\theta - 2\theta_0^0\right)^2\right]^2}, \tag{9}$$

where the dispersion σ_n depends on the dislocation density ρ_n

$$\sigma_n = \frac{f_{hkl}}{2\sqrt{\sqrt{2}-1}}b_n\sqrt{\rho_n}\tan\theta, \tag{10}$$

b_n is the magnitude of Burgers vector of line dislocations, f_{hkl} depends on the Miller indices (hkl) and crystal elastic anisotropy. For a high-nickel alloy [12]

$$f_{hkl} = \frac{2}{1+\nu}\left(1 - 1.65\frac{h^2k^2 + k^2l^2 + l^2h^2}{\left(h^2 + k^2 + l^2\right)^2}\right).$$

In structural materials irradiated at elevated temperatures, Frank interstitial loop growth and unfaulting is occurring and formation of network dislocations is taking place. If the lattice contains both line dislocations and Coulomb type defects, than it would appear reasonable that the X-ray line intensity distribution $I(2\theta)$ is described by a convolution of distribution (Eq. (1)) with that of distribution (Eq. (9)). At $2M \gg 1$, when diffuse X-ray scattering intensity is described by a Cauchy distribution (Eq. (7)), we obtain

$$I(2\theta) = \frac{I_{0i}}{\pi} \frac{2\sigma_n^3}{\left[\sigma_n^2 + \left(2\theta - 2\theta_m^0\right)^2\right]^2} + \frac{I_{1i}}{\pi}\left[\frac{\sigma_c}{\sigma_{cn}^2 + \left(2\theta - 2\theta_m\right)^2} + \frac{2\sigma_n\sigma_{cn}^2}{\left[\sigma_{cn}^2 + \left(2\theta - 2\theta_m\right)^2\right]^2}\right], \quad (11)$$

where

$$\sigma_{cn} = \tfrac{8}{3}\eta_i N|C|\tan\theta + \frac{f_{hkl}}{2\sqrt{\sqrt{2}-1}} b_n\sqrt{\rho_n}\tan\theta. \quad (12)$$

For $2M$ less or not much higher than one, the diffuse scattering intensity distribution must be described by a convolution of the asymmetric distribution with Eq. (9). From the results obtained in Ref. [10], it follows that the approximation error of the asymmetric distribution by Cauchy function (Eq. (7)) does not exceed 2.5%. That is why for all the values of $2M$ the intensity distribution can be represented by Eq. (11). The above-mentioned relationships allow us to determine the concentration, type and size for defects of the Coulomb type and the dislocation line density using the results of XRL profile analysis.

In actual practice, however, analysis of irradiated and deformed materials with complicated profiles involves some problems associated with instrumental broadening and X-ray non-monochromaticity. The measured profile is a convolution of the physical profile, conditioned by the material structure, with the hardware function. The unfolding of the physical profile presents the problem of solving the integral equation of the first kind, whose right side is represented by the measured profile and the integral kernel is described by the hardware function. The REGREN computer code [13] employs the regularization method [14] for physical profile unfolding and employs nonlinear regression analysis for computation of both Bragg reflection and diffuse scattering characteristics.

3. Experiment

Flat specimens of 20Cr–45Ni austenitic alloy were tension-tested at 650°C. Sections of specimens 5×5 mm in area with three deformation levels and one section deformed by rolling at room temperature were subjected to X-ray examination before irradiation. After electropolishing diamond powder was applied on the specimen surface to check the scattering angle. The X-ray patterns were recorded using the diffractometer DRON-2.0 with doublet CuK_α radiation ($\lambda_{\alpha_1} = 1.54051 \times 10^{-1}$ nm) in scanning step 0.01° for (220) and (311), and 0.05° for (420) reflections by scale 2θ. Corresponding reflections from the annealed high-purity nickel are recorded to determine hardware function.

Specimens were irradiated in the fifth row of the BOR-60 reactor in the cell D-23 as components of the irradiation device. Thermocouples and sets of fluence monitors (Ni, Fe, Cu, Nb) were arranged throughout the height of the device. Samples were placed in He-filled stainless steel capsules fixed within the body of the irradiation device at various distances above core midplane and were cooled with sodium. The inlet coolant temperature during the entire irradiation was 325 ± 6°C. The specimen temperature was calculated with knowledge of the inlet coolant temperature and temperature distribution inside the irradiation device. The calculation error was ± 20°C. Sample irradiation conditions are shown in Table 1.

The X-ray study of the irradiated specimens was carried out by means of a remote diffractometer DARD-2. The specimen preparation and the X-ray pattern recording were similar to those used before the irradiation.

After X-ray studies were completed the specimens were mechanically thinned to a thickness of 0.20–0.25 mm. Then 3 mm diameter disks were punched out of these specimens and again mechanically thinned to a thickness of 0.1 mm. The resulting disks were electropolished to

Table 1
Irradiation parameters

Specimen number	Distance above core midplane (mm)	Dose rate ($\times 10^{-7}$ dpa/s)	Dose (dpa)	Temperature (°C)
B1B, B1T, B1M	315	1.9	0.6	400
B2B, B2T, B2M	210	4.6	1.6	400
B3B, B3T, B3M, B3U	0	7.7	2.6	370

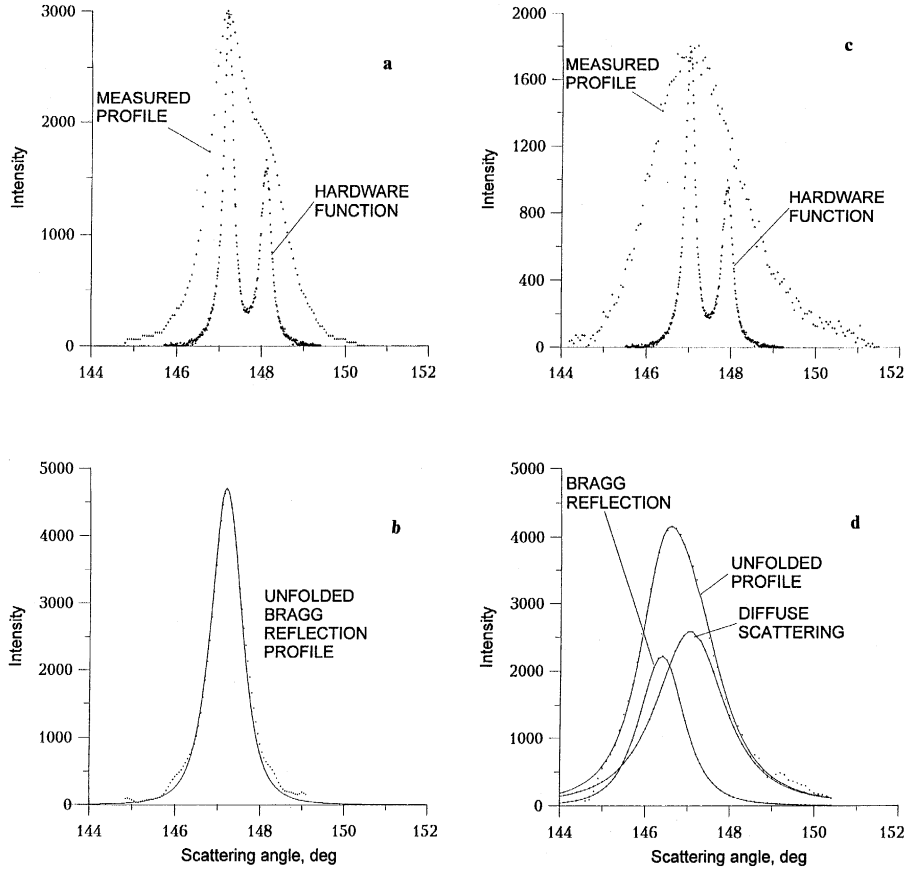

Fig. 2. Measured and unfolded (420) reflection profiles of the B3M specimen (a), (b) before and (c), (d) after irradiation at 7.7×10^{-7} dpa/s.

yield a central perforation. The foils were examined in a EM-125 electron microscope operated at 100 kV. To estimate the network dislocation density, dislocation loops and voids concentration, the foil thickness was taken to be 120 nm. The error in definition of the microstructural values presented in the next section may reach 30–40%.

Table 2
Microstructural parameters in initial and irradiated states of alloy by XRL profile analyses

Specimen number	Lattice parameter (10^{-1} nm)		Network density ($\times 10^{14}$ m^{-2})		$N(\|C\|/a)^{3/2}$ ($\times 10^{-3}$)	NC ($\times 10^{-5}$)	Dislocation loops	
	initial	irradiated	initial	irradiated			density ($\times 10^{22}$ m^{-3})	radius (nm)
B1B	3.5928	3.5910	i 0.5	1.0	0.61	3.8	0.32	19.3
B2B	3.5914	3.5930	0.6	1.7	1.10	6.3	0.45	21.0
B3B	3.5910	3.5954	0.6	2.4	2.20	12.7	0.91	20.8
B1T	3.5920	3.5917	1.4	1.8	0.53	3.5	0.33	18.2
B2T	3.5918	3.5938	1.5	3.4	0.80	5.6	0.59	17.2
B3T	3.5913	– [a]	1.4	4.8	1.45	10.0	1.03	17.4
B1M	3.5895	3.5900	2.2	3.3	0.31	3.1	0.67	12.0
B2M	3.5910	3.5941	2.4	4.5	0.48	4.5	0.85	12.8
B3M	3.5909	3.5980	2.4	6.5	0.74	7.6	1.72	11.7
B3U	3.5933	3.5972	18.5	9.0	0.57	6.3	1.65	10.9

aX-ray pattern recorded without diamond powder.

4. Results

The XRL profile analysis of the deformed and irradiated specimens was performed by the REGREN code. The (420) reflection profiles of the B3M specimen in initial state and after irradiation are shown in Fig. 2. The physical profile before irradiation (Fig. 2(b)) is described by distribution Eq. (9), for which $2\theta_0^0 = 147.19°$, $\sigma_n = 0.66°$. The physical profile after irradiation (Fig. 2(d)), is described by distribution Eq. (11) with the following characteristics:

$I_{0i} = 3.3 \times 10^4$, $\sigma_n = 0.96°$, $2\theta_m^0 = 146.43°$,

$I_{1i} = 6.1 \times 10^4$, $\sigma_{cn} = 1.39°$, $2\theta_m = 147.07°$,

$2M = 1.05$.

Using the position of Bragg reflection peak the lattice parameter of irradiated and non-irradiated specimens was calculated. Using the dispersion of Bragg reflection peak, σ_n, the network density in the initial state was calculated in accordance with Eq. (10). Using the M dependence on $(Qa)^{3/2}$ according to Eq. (3) the values of $N(|C|/a)^{3/2}$ were calculated. Using the shifts of the diffuse scattering maxima, $2(\theta_m - \theta_m^0)$, according to Eqs. (4) and (6) ($\nu = 0.3$) the values of NC were calculated. Using the dispersions σ_n and σ_{cn} in accordance with Eqs. (10) and (12) were calculated the values of $N|C|$ and ρ_n.

The lattice parameter, network dislocation density before and after irradiation, values $N(|C|/a)^{3/2}$ and NC are given in Table 2.

The TEM observation results were used to connect N and C values with the microstructural components. According to these results (Fig. 3) the observable microstructure elements of irradiated specimens are network dislocations, dislocation loops, coherent and non-coherent precipitates of a new phase, and voids. The dominant microstructural components are dislocation loops (Table 3). That is why the values of N and C calculated by characteristics of diffuse scattering should be determined by the loop type, their concentration and sizes. Loops were determined to be interstitial in character because $NC > 0$. Their radius, calculated in account with Eq. (8), and density are given in Table 2.

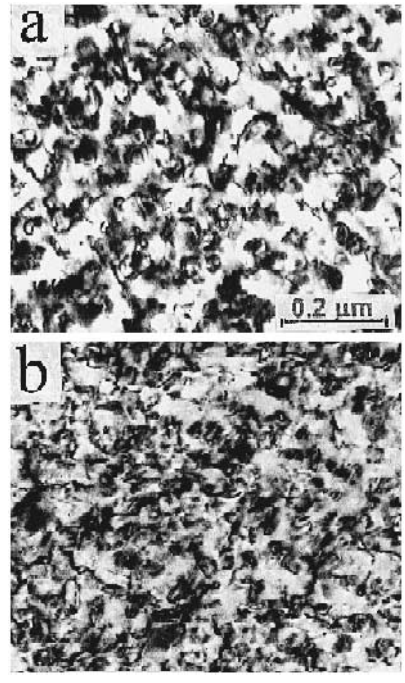

Fig. 3. TEM microstructure of alloy at two initial dislocation densities (a) 0.6×10^{14}, and (b) 2.4×10^{14} m^{-2}, irradiated in BOR-60 at 7.7×10^{-7} dpa/s.

Table 3
Microstructural parameters of irradiated alloy by TEM observations

Specimen number	Network density ($\times10^{14}$ m^{-2})	Dislocation loops		Voids	
		density ($\times10^{22}$ m^{-3})	diameter (nm)	density ($\times10^{20}$ m^{-3})	diameter (nm)
B1B	0.3 [a]	0.28 [b]	22.5 [c]	–	–
B2B	0.9 [d]	0.23	31.5	0.9	10.0
B3B	1.0 [d]	0.75	32.0	1.0	16.0
B1T	2.3	0.08	28.0	–	–
B2T	2.5	0.47	18.0	–	–
B3T	1.3 [d]	0.50	19.0	2.0	14.0
B1M	3.6	– [e]	–	–	–
B2M	3.0	0.39	26.0	–	–
B3M	5.8	0.54	17.0	0.8	12.0
B3U	10.0	0.30	18.0	–	–

[a] Line dislocations decorated by coherent precipitates.
[b] Loops decorated by coherent precipitates; the density is the sum of both loop and coherent precipitate contributions.
[c] Loop diameter is undersized because of contribution of coherent precipitates.
[d] Line dislocations decorated by precipitates.
[e] Density cannot be determined because of loop and coherent precipitate interaction.

5. Discussion

The dislocation loop density as a function of damage rate is shown in Fig. 4. According to X-ray results the loop density is nearly proportional to the square root of the damage rate at 400°C, is higher when the initial network density is higher, and increases with a decrease of irradiation temperature. The dose-rate dependence provides evidence that the loop density reaches a saturation level within the examined doses, and the nucleation of interstitial loops occurs by a reaction between free interstitials and not by cascade collapse [15]. The dependence on initial network density corresponds to the idea that the interstitial loop nucleation is more probable, if at the start of irradiation, there are sinks for interstitial point defect.

The scatter of the TEM measurements does not allow us to determine the loop density dependence on the initial network density. The loop density, defined by various methods is rather close for specimens with low network density, but if ρ_n increases, the loop densities determined by TEM are several times lower than that determined by XRL profile analysis. The discrepancy between the two methods can be explained in the following way. Loop density defined by XRL profile analyses may be overestimated because of the contribution of coherent precipitates in diffuse scattering characteristics. The possible scatter in TEM observations may arise from the local heterogeneity of the dislocation structure and the foil thickness error. The lower loop density determined by TEM observations may be connected with the resolution limitation at high total dislocation density.

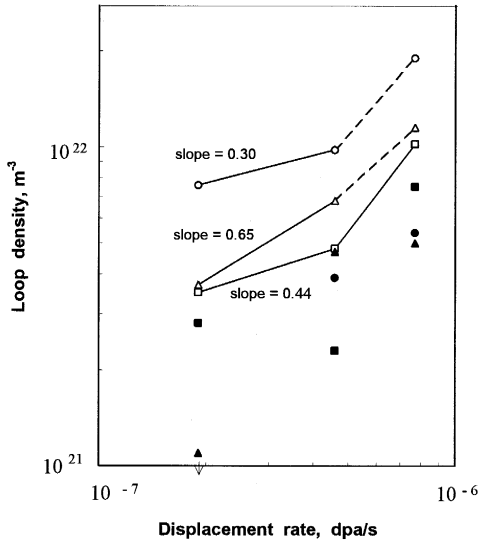

Fig. 4. Dependence of dislocation loop density on displacement rate for various initial network densities (□, ■) 0.5, (△, ▲) 1.4, (○, ●) 2.4×10^{14} m^{-2}. Open and filled symbols denote X-ray and TEM results, respectively. The indicated slopes correspond to a dependence for an irradiation temperature of 400°C.

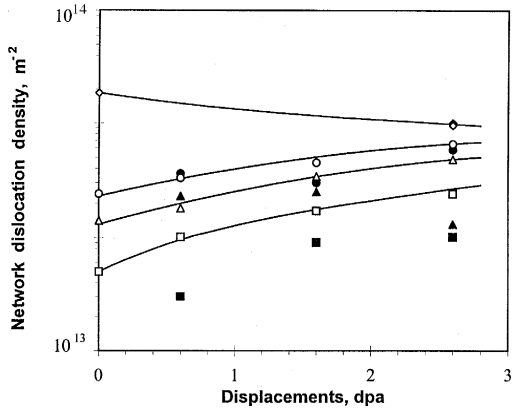

Fig. 5. Network dislocation density evolution as revealed by the results of XRL profile analysis and TEM observations. Symbols are the same as in Fig. 4.

The results presented in Tables 2 and 3 show that loop sizes, determined by XRL profile analysis, are a bit higher than those determined by TEM observations. The loop radius does not appear to depend on irradiation parameters and probably is determined by the initial network density.

Independent of the initial dislocation level, the network density tends toward a saturation density in the range from 6 to 9×10^{14} m^{-2} with increasing dose (Fig. 5). This tendency corresponds to the general trend of microstructural evolution observed in Fe–Cr–Ni alloys irradiated up to high doses: the saturation dislocation density lies in the band $(6\pm3)\times10^{14}$ m^{-2}, relatively independent of the starting state, displacement rate and other variables [16]. The noticeable difference of the XRL profile analysis and TEM results at low initial dislocation density and the rather good agreement at $\rho_n > 3\times10^{14}$ m^{-2} may arise from the method of foil preparation for TEM observation. Upon mechanical thinning of specimens, glide and annihilation of the unpinned line dislocation segments is possible, and correspondingly may lead to the observed decrease of the dislocation density. As the network density increases, the pinned dislocation segment fraction increases and that may explain the coincidence of XRL profile analysis and TEM results.

6. Conclusion

According to the theory of X-ray scattering by imperfect crystals, procedures and software were developed to allow the microstructural study of irradiated and deformed materials using XRL profile analysis.

The dislocation structure of the predeformed specimens of a 20Cr–45Ni alloy, before and after irradiation at three displacement rates, was studied by XRL profile analysis and TEM observation.

The joint application of those two methods provided a rather high accuracy of results and allowed us to define

possibilities of both techniques. In the electron microscope a broader spectrum of radiation-induced defects is observed. The XRL profile analysis provides the more higher accuracy for determining dislocation structure parameters.

Using those methods, we have defined the dependence of dislocation loop density and network density on irradiation conditions and the initial state, and found them to be consistent with the results of other studies.

The results obtained can be used for prediction of microstructural changes at higher irradiation doses.

Acknowledgements

The authors are very much obliged to the members of the X-ray analysis group under the leadership of Professor V.M. Kosenkov for obtaining the X-ray pattern records. The authors would like to express their gratitude to Dr F. Garner for very useful discussion and helpful comments on the first version of of this manuscript.

References

[1] M.L. Grossbeck, K. Ehrlich and C. Wassilew, J. Nucl. Mater. 174 (1990) 264.
[2] F.A. Garner, H.L. Heinisch, R.L. Simons and F.H. Mann, Radiat. Eff. 113 (1990) 229.
[3] H.R. Brager, L.D. Blackburn and D.L. Greenslade, J. Nucl. Mater. 122&123 (1984) 332.
[4] L. Le Naour, N. Vouillon and V. Levy, in: Effects of Radiation on Materials, eds. H.R. Brager and J.S. Perrin, ASTM-STP, Vol. 782 (1982) p. 310.
[5] M.A. Krivoglaz, Theory of X-Ray and Thermal Neutron Scattering by Real Crystals (Plenum, New York, 1969).
[6] H. Oettel, Phys. Status Solidi (a)6 (1971) 265.
[7] A.N. Ivanov, Freiberg. Forschungsh. 265 (1988) 95.
[8] A.A. Katznelson, Yu.D. Goncharenko, R.B. Grabova et al., Fiz. Metal. Metalloved. 51 (1981) 794.
[9] A.A. Katznelson, Yu.D. Goncharenko, R.B. Grabova et al., Fiz. Metal. Metalloved. 49 (1980) 1256.
[10] R.I. Barabash and M.A. Krivoglaz, Fiz. Metal. Metalloved. 45 (1978) 7.
[11] J.M. Burgers, Proc. K. Ned. Akad. Wet. 42 (1939) 293.
[12] R.B. Grabova, Yu.D. Goncharenko, V.K. Gorbatov et al., Fiz. Metal. Metalloved. 61 (1986) 1164.
[13] R.B. Grabova, in: Hardware and Methods of X-Ray Analysis, Vol. 37 (Mashinostroenie, Leningrad, 1988) p. 79.
[14] A.N. Tikhonov and V.Ya. Arsenin, Methods of Ill-Posed Problems Solving (Nauka, Moscow, 1974).
[15] N. Yoshida, J. Nucl. Mater. 205 (1993) 344.
[16] F.A. Garner, J. Nucl. Mater. 205 (1993) 98.